PUBLICATIONS OF THE ASTRONOMICAL SOCIETY OF THE PACIFIC, **125**:1015–1020, 2013 August

Ghost Image Correction in CSTAR Photometry

ZEYANG MENG,[1] XU ZHOU,[2] HUI ZHANG,[1] JILIN ZHOU,[1] SONGHU WANG,[1] JUN MA,[2] TIANMENG ZHANG,[2] ZHOU FAN,[2] AND HU ZOU[2]

Received 2013 May 15; accepted 2013 June 21; published 2013 July 26

ABSTRACT. During the Polar Night of 2008 at Dome A site (Antarctica), the Chinese Small Telescope ARray (CSTAR) gathered i-band photometric information (a total of over 300,000 images) of the 20 deg^2 sky vicinity around the South Pole automatically and continuously. Within all the acquired images, we carry out an elaborate series of analyses and study the origin and influence of the ghost images in each frame. The point source catalog has also been amended by removing the ghost image effects from the real overlapped stars. This work provides a generalized ghost reduction pipeline and improves the photometric precision of the stars in the CSTAR FOV for the future search for transiting exoplanets.

Online material: color figure

1. INTRODUCTION

Transiting exoplanet searching requires long observational baseline and high photometric precision. However, due to the spin and atmosphere of the Earth, it is difficult to satisfy these requirements on the ground at the same time. Several space program have achieved high quality, like *CoRoT* (Baglin et al. 2006) and *Kepler* (Borucki et al. 2010). While the cost of space programs is too high for us, the Antarctic plateau offers an alternative option on Earth to obtain similar observations with lower costs. An ideal site, the Antarctic plateau has the coldest and driest air (absolute water vapour value) above the continent (Burton 2010), which is best for wavebands like optical, infrared and submillimeter (Lawrence 2004), and the thin atmosphere layer makes the atmosphere even more stable and less turbulent (Bonner et al. 2010). Moreover, another advantage of the Antarctic plateau is the coherent time series of the polar night, which is superior for transit search (Rauer et al. 2008).

These specialities of the Antarctic plateau have attracted many astronomical projects just in the past 30 years (see a historical summary in Indermuehle et al. [2005]). The first optical research program started in 1980 (Grec et al. 1980) and from then on, many scientific products appeared in various astrophysical fields (see Burton [2010] and references therein). Take high accuracy photometry for example; the ASTEP project has carried out several pioneering works at Dome C site, such as the first evidence for a secondary eclipse acquired by a ground-based observation (Abe et al. 2013) following the site-testing and characterization of transiting exoplanet detection limits by Crouzet et al. (2010).

Dome A, located at $80°37'S$ and $77°53'E$, has a special position in Antarctic astronomy, since it is the highest site in Antarctica (with an elevation at 4093 m). After comparing cloud cover, boundary layer thickness, seeing, and so forth, Saunders et al. (2009) pointed out that Dome A could potentially be the best site on Earth. The Chinese Center for Antarctic Astronomy (CCSS) has successfully launched CSTAR there (as will be described in § 2). It is a great opportunity and yet a tremendous challenge in technology and implementation. So far many endeavors have been undertaken and it is worth mentioning some works like the first catalog released by Zhou et al. (2010a) and sky brightness and transparency analysis by Zou et al. (2010). Recently, the photometric precision has been twice improved by Wang et al. (2012, 2013) after considering the inhomogeneous effect of cloud cover and diurnal effect. From previous works we find out that ghost images effect is another important issue concerning photometric precision.

Ghost images are not rare in optical system, especially in the case of large field Schmidt telescopes. U.K. Schmidt Telescope Unit (UKSTU) classified ghost images into five cause-related types: emulsion-corrector, filter-corrector, corrector, filter, and spike ghosts. In design, CSTAR also has a Schmidt-Cassegrain optical structure, so ghost images can occur in the field of CSTAR. The UKSTU Handbook (1983) describes ghost images of this type as a diffuse spot located opposite to the bright primary star with respect to the optical symmetric axis (or optical axis). The process of ghost image correction is of fundamental importance because ghost images can not only be mistaken for normal stars in aperture photometry, but also overlap on real stars and cause extra photometric noise. To remove this instrumental effect, we first confirm the most significant ghost "producer" (some

[1] Department of Astronomy of Astronomy and Key Laboratory of Modern Astronomy and Astrophysics in Ministry of Education, Nanjing University, Nanjing 210093, China.

[2] National Astronomy Observatories, Chinese Academy of Sciences, Beijing 100012, China; zhouxu@bao.ac.cn.

of the bright stars). Then we can find the optical axis of these ghost images and bright stars. Finally, by removing the ghost image and its influence on real stars, we get a renewed catalog.

In this paper, we describe optical design and previous data reduction of CSTAR in § 2. Then in § 3, we describe the causation and correct methodology of ghost images, while primary results and discussion of our ghost correction is presented in § 3. Conclusions are presented in § 4.

2. THE OPTICAL DESIGN OF CSTAR AND PREVIOUS DATA REDUCTION

Deployed as a part of the PLATO (Lawrence et al. 2009; Yang et al. 2009), CSTAR telescope was designed by Nanjing Institute of Astronomical Optics & Technology (NIAOT), embedded in Antarctic Dome A and pointed fixedly at the South Celestial Pole. CSTAR consists of 2×2 telescopes, and each telescope has a different SDSS band, namely: g, r, i, and an open band. With an effective field of view (FOV) of about $4.5° \times 4.5°$ (20 $\deg^2$), CSTAR is equipped with an imaging device, Andor DV435 $1\ \mathrm{k} \times 1\ \mathrm{k}$, whose pixel size corresponds to $15''$ sky angle (Yuan et al. 2008). The internal optical structure of the CSTAR telescope is illustrated in Figure 1. Technically, the SDSS i-band filter was coated on the front surface of the corrector, while an extra reflective silver film was coated on the right surface of the secondary mirror. A ghost image is very likely to be produced when stellar light is reflected between these two coated surfaces.

After being transported to Dome A in 2008 January, CSTAR was successfully settled. However, during the first observation season, only the i-band of worked well and a total of over 310,000 images with integration times of 20 or 30 s were taken between 2008 March 4 and August 8 during the polar night of Dome A site. These images exhibit a detailed continuous observation around the South Celestial Pole of total exposure as long as 1728 hr.

Once the raw data was fetched back, two groups have done their own data analysis work. Zhou et al. (2010a) published a catalog of more than 10,000 CSTAR Point Sources and calculated sky brightness and transparency conditions in the i-band of Dome A site. Later, Wang et al. (2011) released 157 variable stars, six times the number of previous observations. Most recently, Wang et al. (2012) improved the catalog's photometric precision by considering the effect of inhomogeneous clouds. This work on ghost image correction is based on the catalog given by Wang et al. (2013) after removing the diurnal effects.

Here we briefly mention Zhou's work: Zhou et al. (2010a), after applying some preliminary image reductions, conducted aperture photometry for all the frames with three different aperture radii: 3, 4 and 5 pixel size. Then a frame with good photometric condition was used as standard image for calibrating magnitude offsets, and for the other frames they used a pattern match among the selected bright stars to get regularized positions (master coordinates) for the standard frame. Finally, a comparison and calibration between 48 CSTAR field stars and USNO-B1.0 system gave us the released catalog.

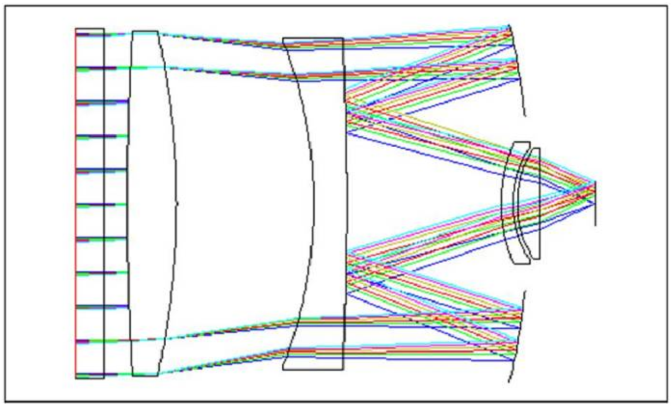

FIG. 1.—Optical design of CSTAR, which is constructed with multi-mirror structure. The first plano lens serves as corrector (*right part*) and filter (*left part, larger than the physical size*) while the *rightmost* reflective layer with an inner hole acts as the primary spherical mirror. The right surface of the middle component mirror is coated with reflective film. This picture is taken from Zhou et al. (2010b). See the electronic edition of the *PASP* for a color version of this figure.

3. GHOST IMAGES AND CORRECTION IN CSTAR

3.1. Ghost Images in CSTAR

Since CSTAR was fixed to the ice sheet and pointed toward the vicinity of the South Celestial Pole (Pole hereafter), star spots move clockwise on CCD due to diurnal motion. The rotational angle of this circular motion with respect to a chosen image ('A5CH5029', the standard frame) in each frame can be measured during the stellar pattern match procedure. Hence, the same star in different images can be identified and normalized to its coordinates in standard frame (viz. the master coordinate). We know that ghost images (false stars) are located symmetrically opposite to bright stars and the optical symmetric axis doesn't overlap with the South Celestial Pole on CCD. While the same stars in different images are matched with the standard frame, ghosts will never match with themselves until a sidereal day. After stacking all the images within a day and technically masking all the confirmed stellar spots out, we can get a whole-day dirty stack, where ghost images produce some circles (see Fig. 2). As we can infer, ghost images which move opposite to the stars could encounter real stars periodically. Taking the slight motion of the glacier where CSTAR was fixed into account (Zhou et al. 2013), stellar spots can wobble, and therefore ghost images might overlap with several real stars in a day and consequently cause stellar magnitude decrease by a maximum of ~1.0 (shown in Fig. 3). This kind of change in brightness can be mistaken as a false physical property of these real stars. So it is of great necessity to rectify these kind of instrument-induced cyclic effects for high photometric demanding future works like transiting exoplanet search.

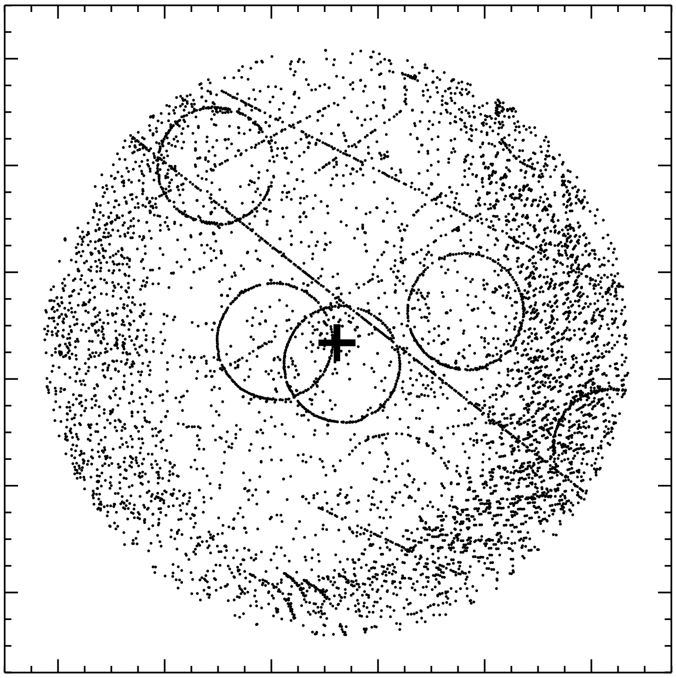

FIG. 2.—A whole day's frames stack (*dirty stack*). *Circles* (*or arcs*) are ghost image patterns. The *black cross* marks the South Pole. For a better view, we have removed the confirmed real stars in the field.

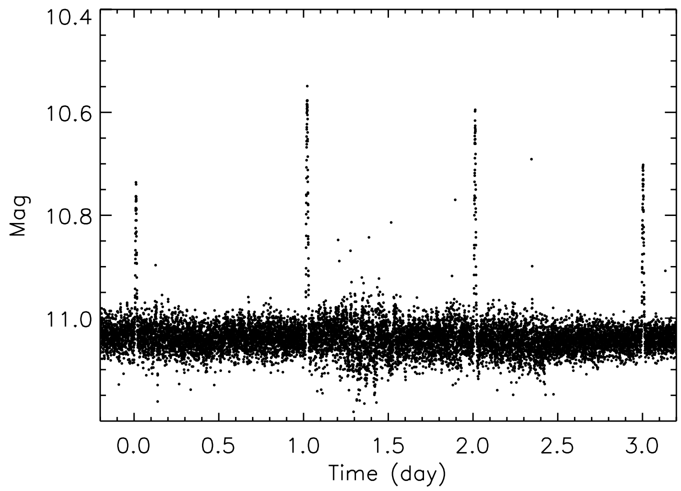

FIG. 3.—The light curve of an arbitrarily chosen real star (R.A.: $23^h24^m28.4^s$, decl.: $-89°25'10.6''$). Typically, a certain ghost image overlaps with the real star once within a sidereal day and consequently causes the real star's magnitude to brighten by approximately half a magnitude.

3.2. Ghost Correction in CSTAR

To remove the additional flux contributed by ghost images of the real stars, we need to identify ghosts' progenitors (i.e., the bright source stars) instead of simply using photometric magnitudes of ghost images to correct the real stars, because ghost images are most commonly extended faint sources and aperture photometry would get contaminated by noise and become unreliable. Another important process is to determine how much the magnitudes of the affected stars vary with time. Once we do this, we can amend the CSTAR catalogs and renew them.

Practically, we developed a pipeline to identify ghost patterns and eliminate the impact on these contaminated stellar flux. In brief, the method contains three steps:

1. Determine location of optical axis and ghost sources. In the crowed stellar field of CSTAR, we are unable to search for every ghost image on every single frame. So we determine the locations and radii of the most predominant ghost rings in the dirty stack. Meanwhile, the limiting magnitude of the telescope leads to the fact that only the brightest stars can produce ghost patterns. When we match the centers of the ghost rings with the top 100 brightest stars, the matched ones are the ghost source stars (source stars or producers). Once the list of the ghost producers is built up, we search each frame for master coordinates [*X*, *Y*] of ghost images which are in the ghost rings to get ghost image candidates. Finally, local coordinates [*x*, *y*] of these candidates are used to link with the corresponding source stars to get a series of lines. Then we cross these lines with each other to get the intersections, which are the optical symmetric axis pixel values on CCD.

2. Find the quantitative influence of ghost images on real stars. As we get the optical symmetric axis coordinates on CCD, the magnitudes and locations of ghost source stars and ghost images can both be retrieved from Wang's catalog (Wang et al. 2012). Then we can measure how the magnitude of real stars changes as the ghost image approaches or overlaps them. Let us denote d as the pixel distance between a real star and ghost image, while $\mathrm{mag_{src}}, \mathrm{mag_{ghost}}, \mathrm{mag}_s^0$, and mag_s^1 are the magnitudes of the source star, ghost image, and the same star unaffected and affected by the ghost. There are two basic assumptions in this step: One is $F_{\mathrm{ghost}} = f_0 \cdot F_{\mathrm{src}}$, which means a fraction (say f_0) of the producer's (or source's) flux was reflected and counted into the corresponding ghost image's flux; the second is $\delta F_s = F_{s,\mathrm{affected}} - F_{s,\mathrm{unaffected}} = f_1(d) \cdot F_{\mathrm{ghost}}$, which means a fraction (for example, f_1, which is a function of distance) of the ghost's flux was counted into the real star which was being affected. After applying the definition between magnitude and flux: $m = -2.5 \lg F + m_0$ to these two assumptions, we get the following relations:

$$\begin{cases} \mathrm{mag_{ghost}} = -2.5 \lg f_0 + \mathrm{mag_{src}} \\ f_1(d) \cdot f_0 \cdot C^{\mathrm{mag_{src}}} = C^{\mathrm{mag}_s^1} - C^{\mathrm{mag}_s^0} \end{cases} , \quad (1)$$

where $C = \lg 2.5$. In a statistical way, we can gather all the confirmed ghosts, source stars, and affected stars to estimate the two fundamental parameters: f_0 and f_1. It is necessary to mention that the ghost image from each bright source differs from the others in these two parameters. So here we normalize $f_1(d)$ to one unit for convenience.

3. Correct the catalog. Following previous step, when we get the needed reflected parameter f_0 and magnitude distance relation parameter $f_1(d)$, for a certain frame taken at time t, the real star's magnitude correction value $\delta\mathrm{mag}_s(t, d, \mathrm{mag}_s, \mathrm{mag}_{\mathrm{src}})$ can be calculated and applied to the catalog. Thus we can get an updated catalog without ghost effects.

4. RESULT AND DISCUSSION

After fitting the radii (approximately 107 pixels) and centres of the ghost rings, and by matching[3] the ghost rings' centres to the reference catalog (Wang et al. 2012), we can get a preliminary list of the producer candidates. To get a complete catalog of the ghost source stars, we need to evaluate the magnitude difference between these matched producers and the corresponding ghost stars ($\delta i \approx 5.5$, see Fig. 6); and when considering the limiting magnitude ($i \approx 14.0$) given by Wang et al. (2012), we know that stars with $i \leq 8.5$ need to be classified into the candidate source stars.

However, the truth is not all stars with magnitude brighter than 8.5 are ghost generators, since several factors determine whether these bright stars can produce ghost images. The most important two factors are the locations of the bright stars relatively to the center of FOV and the distances between these stars and the optical axis. The reason is that if a certain bright star is located too far from the center of CSTAR's FOV or optical axis, it will be a long optical path before the reflected star light could get outside the reflecting mirror layers, and the longer it takes, the fainter and less important the ghost image would be.

Once we have the complete catalog, we link the ghost source stars with every star that is covered by the ghost rings and get the histogram distribution of the optical axis on CCD. As we can see Figure 4, optical axis' local pixel coordinates are $[477 \pm 2, 297 \pm 2]$. This value is tested under the real image (Fig. 5). Considering the geometry between the ghost ring and producers, we can easily get a relation between the ghost ring's radius and the distance of the Pole and optical axis:

$$r_{\mathrm{ghost}} = 2 \cdot d_{\mathrm{Pole,axis}}. \quad (2)$$

Substituting the coordinates of the Pole (i.e., [523, 467]) and optical symmetric axis (i.e., [477, 497]) into equation (2), we calculate that ghost ring radius is 109 pixels, which is consistent with the previous fitting value (107 pixels).

As for the first impact parameter f_0, Figure 6 illustrates that the ghost image changes with almost the same tendency, and the difference between the producer's magnitude and the ghost image's magnitude is about 5.4, which means about 0.7% of the bright producer's flux was reflected and converted into ghost's flux. However, we should also realise that for each ghost image, the situation is even more complicated: Different ghost

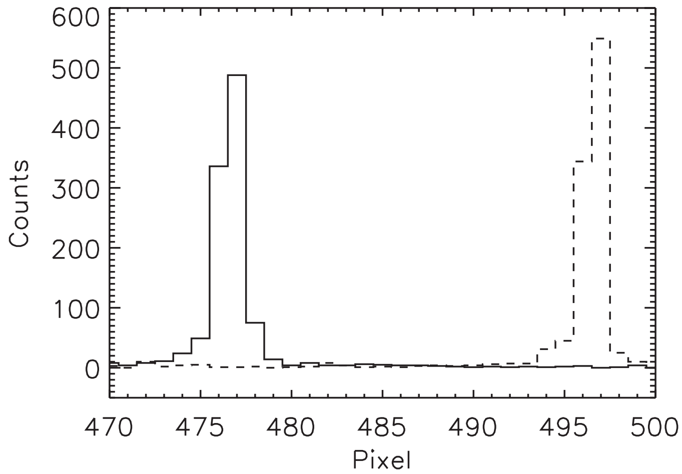

FIG. 4.—Histogram counts of optical symmetric axis on CCD. The *solid line* stands for the *x* local pixel value while the *dashed line* stands for *y*. The binsize of each histogram is one pixel.

sources' locations and magnitudes can introduce additional uncertainties of f_0.

When working with the second parameter, we're assuming every ghost's flux is 0.7% of the corresponding producer's. Here we give an example (shown in Fig. 7). It is natural to treat the function as a Gaussian profile; because ghost images are usually an extended source, real stars can only be influenced when the distance between the two is smaller than the ghost radius. We have done a Gaussian fitting of the function, which is normalised as below:

$$f_1(d) \simeq A_0 \cdot e^{-Z^2/2} \quad , \quad (3)$$

where $Z = (d - A_1)/A_2, A_0 \approx 0.97, A_1 \approx -0.86,$ and $A_2 \approx 2.99$. Here we have to say it is even more difficult to

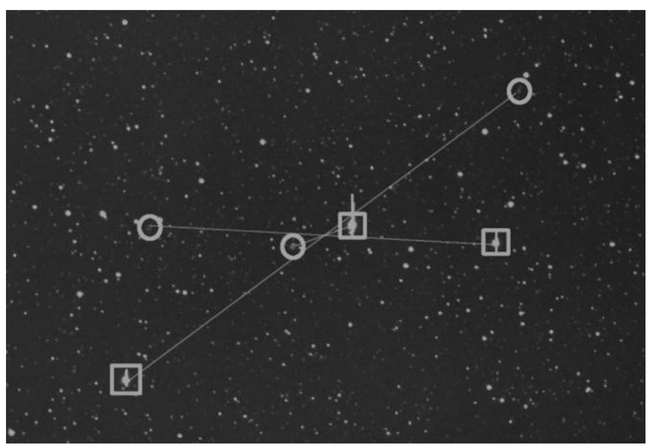

FIG. 5.—Optical symmetric point on a chosen image "16RE0312.fit". Bright blended source stars are in *squares* and corresponding ghost images are in *circles*. *Solid lines* between them intersect at the optical symmetric point.

[3] Please see http://spiff.rit.edu/match/.

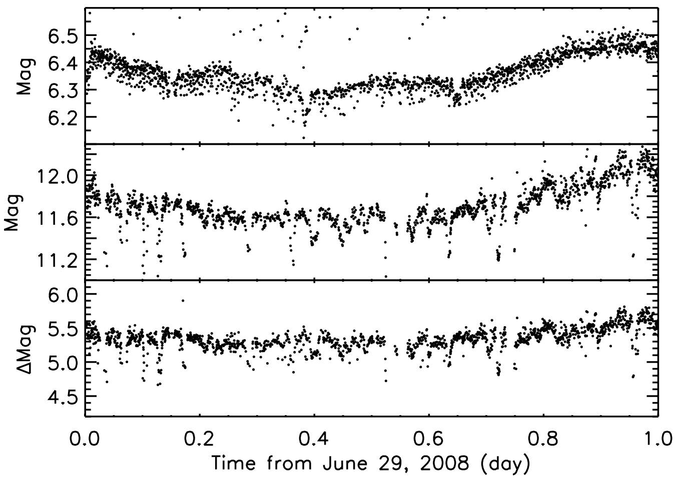

FIG. 6.—*Top panel* describes one-day magnitudes of a ghost source star (R.A.: $21^h08^m44.2^s$, decl.: $-88°57'21.6''$). *Middle panel* shows magnitudes of the ghost image produced by the upper source star within a day. *Bottom panel* is the magnitude difference between upper two light curves.

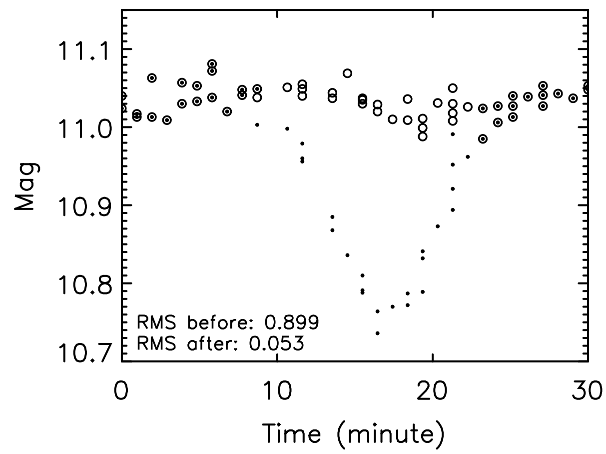

FIG. 8.—Comparison between the light curves of a star (R.A.: $23^h24^m28.4^s$, decl.: $-89°25'10.6''$) before (*dots*) and after (*open circles*) ghost correction. As shown, corrections will immediately be applied as long as a ghost image overlaps with the real star within a certain radius, and therefore a substantial improvement of light curve's rms can be achieved.

measure $f_1(d)$, because the true magnitude of the real star cannot be estimated when it is overlapped by ghost. What we do is treat the real star's magnitude as a constant value, which is the master magnitude given by Wang et al. (2012). The upper relation also implies that the typical radius of a ghost image is roughly 6 pix, which is larger than photometric apertures (Zhou et al. 2010a). On one hand, this proves that we cannot simply use the photometric magnitude of the ghost image to correct the influenced real star, while on the other hand it confirms that parameter f_0 may induce extra uncertainties.

The last step is subtracting the ghost's residual from the effected star's magnitude. Using relations that have already been

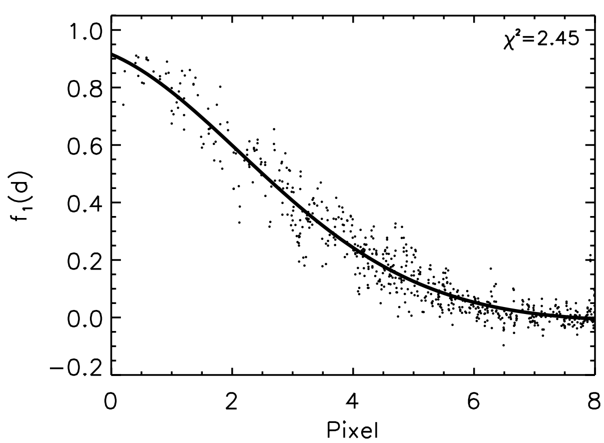

FIG. 7.—Relation between ghost-impact parameter $f_1(d)$ and distance measured between the moving ghost image and the real star. *Black solid line* is Gaussian fitting given by equation (3). When the distance between the ghost image and real star is larger than ~6 pixels, no influence of ghost image acts on the real star, whereas up to 97% of the ghost's flux is counted into the real star's flux when totally superposed.

deduced, we can determine when and where the ghost begins to overlap with the real star, and thus update the catalog without major ghost's effect. An example (Fig. 8) shows that our correction is effective within stellar photometric error, even though the stellar location is not well restrained within a 2 pixel radius.

5. CONCLUSION

Owing to the unique advantages of the Antarctica Plateau, CSTAR has reached many scientific achievements. Thanks to its large FOV and long observation sequence, it is feasible to continue with several scientific follow-up programs (like transiting planet search, which requires high photometric precision and high cadence) with some photometric corrections. After the observing season finished in 2008, data were retrieved from Dome A site and since then the first version catalog was released (Zhou et al. 2010a) and updated by Wang et al. (2012, 2013) afterwards.

In this work, to achieve higher photometric precision of stars in CSTAR field, we investigate the internal structure of the telescope, find out the principle of the ghost cause and effect factors, evaluate the impact parameters of ghost images, correct the ghost effects within the catalog, and update the whole catalog with an overall photometric accuracy improvement (magnitude correction value upto 0.6 mag and light curve rms improvement from 0.9 to 0.05 within the ghost affected interval), which could pave the way for future transiting exoplanet search and data reduction processes of future Antarctic telescope generations like AST3 (Cui et al. 2008). The updated catalog will be accessible online.[4]

[4] Please see http://archieve.bao.ac.cn/en/cstar.

This work has been supported by the National Basic Research Program of China (No. 2013CB834900), the National Natural Science Foundation of China under grant No. 11073032, 10925313, 10833001, The National Natural Science Funds for Young Scholar (No. 11003010). We are also grateful to High Performance Computing Center (HPCC) of Nanjing University for the catalog refinement process.

REFERENCES

Abe, L., Gonçalves, I., Agabi, A., et al. 2013, A&A, 553, A49
Baglin, A., Auvergne, M., Boisnard, L., et al. 2006, 36th COSPAR Scientific Assembly, 36, 3749
Bonner, C. S., Ashley, M. C. B., Cui, X., et al. 2010, PASP, 122, 1122
Borucki, W. J., Koch, D., Basri, G., et al. 2010, Science, 327, 977
Burton, M. G. 2010, A&A Rev., 18, 417
Crouzet, N., Guillot, T., Agabi, A., et al. 2010, A&A, 511, A36
Cui, X., Yuan, X., & Gong, X. 2008, Proc. SPIE, 7012, 83
Grec, G., Fossat, E., & Pomerantz, M. 1980, Nature, 288, 541
Indermuehle, B. T., Burton, M. G., & Maddison, S. T. 2005, PASA, 22, 73
Lawrence, J. S. 2004, PASP, 116, 482
Lawrence, J. S., Ashley, M. C. B., Hengst, S., et al. 2009, Rev. Sci. Instrum., 80, 064501
Rauer, H., Fruth, T., Erikson, A. 2008, PASP, 120, 852
Saunders, W., Lawrence, J. S., Storey, J. W. V., et al. 2009, PASP, 121, 976
UKSTU Handbook 1983 (Edinburgh: Royal Observatory)
Wang, L., Macri, L. M., Krisciunas, K., et al. 2011, AJ, 142, 155
Wang, S., Zhou, X., Zhang, H., et al. 2012, PASP, 124, 1167
Wang, et al. 2013, in press
Yang, H., Allen, G., Ashley, M. C. B., et al. 2009, PASP, 121, 174
Yuan, X., Cui, X., Liu, G., et al. 2008, Proc. SPIE, 7012, 152
Zhou, X., Ashley, M. C. B., Cui, X., et al. 2013, in IAU Symposium 288, Astrophysics from Antarctica, ed. T. Montmerle, I. Corbett, U. Grothkopf, & C. Sterken (New York: Cambridge), 231
Zhou, X., Fan, Z., Jiang, Z., et al. 2010a, PASP, 122, 347
Zhou, X., Wu, Z.-Y., Jiang, Z.-J., et al. 2010b, Res. Astron. Astrophys., 10, 279
Zou, H., Zhou, X., Jiang, Z., et al. 2010, AJ, 140, 602